CLIMA 2016 - proceedings of the 12th REHVA World Congress

volume 5

Heiselberg, Per Kvols

Publication date:
2016

Document Version
Publisher's PDF, also known as Version of record

Influence of Thermal Boundary Conditions on the Entrainment Behavior of an Active Chilled Beam

Henning Freitag[#1], Paul Mathis[#2], Dirk Müller[#3]

[#]*E.ON Energy Research Center, Institute for Energy Efficient Buildings and Indoor Climate, RWTH Aachen University*
Mathieustr. 10, 52074 Aachen, Germany

[1]hfreitag@eonerc.rwth-aachen.de

[2]pmathis@eonerc.rwth-aachen.de

[3]dmueller@eonerc.rwth-aachen.de

Abstract
An experimental setup used to study the effect of varying thermal boundary conditions on the entrainment behavior of an active chilled beam (ACB) is introduced in detail. Thermal power and entrainment ratio are measured simultaneously for temperature differences between water supply and secondary air ranging from 5 K to 15 K representing different cooling temperature potentials of the heat sink. For constant secondary air temperatures entrainment ratios decrease with increasing water supply temperature. However, effects are small over the temperature range investigated in this study. It is concluded that geometry adjustments of the ACB are not required in order to maintain the desired entrainment ratios in cases when water is supplied at a higher temperature, for example when using a geothermal heat sink. Reproducibility of measurements of the thermal power and the entrainment ratio is dependent on ambient air conditions and is quantified as below 1% and below 2% of the measured value, respectively. Average repeatability of measurement results is below 0.5% of the measured value.

Keywords - active chilled beam; non-isothermal; entrainment

1. Introduction

Active chilled beams (ACB) are used to simultaneously ventilate and cool or heat indoor spaces. The characteristic feature of these devices is the entrainment of air due to turbulent mixing at the jet edges of multiple small, high velocity primary air jets which are located inside the device. This entrainment causes room air to be drawn into the chilled beam where it is cooled or heated according to the occupants' needs by passing a heat exchanger with a set water temperature. The thermal power of the active chilled beam is determined by the entrainment ratio (or induction ratio) $I_e = \dot{m}_{sec}/\dot{m}_{prim}$ meaning the ratio between the mass flow rate of the entrained secondary air $\dot{m}_{sec}$ and the supplied primary air $\dot{m}_{prim}$. The entrainment ratio is mainly determined by geometrical influences such as the nozzle design and the internal wall contour of the device as well as the flow

resistance of the heat exchanger. However, the flow pattern is also influenced by the fluid's local density distribution which is variable when the active chilled beam is operated under non-isothermal conditions, as in the cooling or heating mode.

Many investigations on free-shear flow, particularly on jets and their entrainment behavior can be found in the literature [1][2]. However, few address non-isothermal flow conditions meaning that a temperature difference between the jet and the surrounding fluid is altering the flow pattern. Entrainment behavior of a turbulent, round viscosity-stratified jet has been investigated by Chhabra et al [3] for different viscosity ratios between the jet fluid and the surrounding fluid at equal densities.

In order to understand the relevant physical effects better the general characteristics of the internal air flow of a fixed, generic ACB geometry with multiple nozzles and without heat exchanger have been investigated under isothermal conditions in an experimental study by Freitag et al. [4] and in a simulative study by Koskela et al. [5].

In this paper, the influence of the thermal boundary conditions on the entrainment behavior of an active chilled beam is investigated experimentally by measuring the entrainment ratio and the thermal power of the chilled beam simultaneously. Measurement data is used to gain information on how higher water supply temperatures require optimized beam geometries, e.g. when using geothermal heat sources for indoor cooling which has been discussed in Mathis et al. [6].

2. Methods

2.1 Experimental setup

Measurements were conducted using an experimental setup containing a typical active chilled beam for office applications mounted in an artificial suspended ceiling. For usability reasons ceiling and ACB are installed in an upturned position approx. 0.7 m above the floor of our laboratory. A schematic of the experimental setup is displayed in Fig. 1. Two variable speed centrifugal blowers are used to supply primary and secondary air to the ACB in separate ducts. The respective flow rates are determined using circular orifice plates and high accuracy pressure sensors (Sensirion SDP2000-L) using the differential pressure method. Rotational speed of the primary air blower is controlled according to the set volumetric flow rate.

In order to ensure that only the measured secondary air mass flow is entrained by the ACB a custom-made hood is placed on top of the ACB inlet and is made airtight against the ambience. The rotational speed of the secondary air blower is controlled in order to maintain a static pressure difference of $\Delta p = p_{sec} - p_{amb} = 0$ between the secondary air and the ambient air. The pressure difference is measured using a suitable differential pressure sensor (Sensirion SDP1000-L025) which is connected to an annular

tube including six pressure measurement taps in the outer wall of the secondary air hood at a height of 50 mm above the ACB inlet. Several layers of perforated sheet and fleece mat are used to ensure an evenly distributed velocity profile of the secondary air flow approaching the ACB.

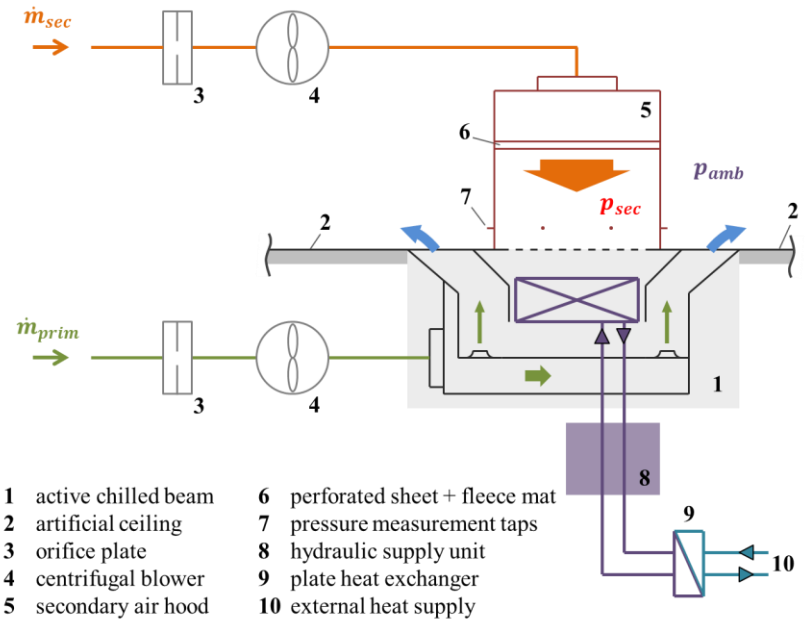

Fig. 1 Schematic of the experimental setup

The ACB's heat exchanger is connected to a hydraulic supply unit in order to be able to adjust its thermal power. A schematic of the unit is displayed in Fig. 2. The water mass flow $\dot{m}_{water}$ is measured by an electromagnetic flowmeter (Krohne Optiflux 5300) and is altered by controlling the speed of the circulating pump. A magnetically actuated mixing valve (Siemens MXG461) is used to adjust the water supply temperature accurately to the desired value by leading a fraction of the water over a plate heat exchanger that is connected to an external heat supply. Depending on the desired operating mode of the ACB, the external heat supply can be used to adjust ACB heat exchanger supply temperatures in a temperature range between 12 °C and 60 °C, either as a constant absolute value or a constant temperature difference value, to account for changing ambient conditions, for example.

All set values are controlled automatically in order to obtain good reproducibility of the measurements using industrial controlling hardware

(ICP DAS ET-87Pn series components) and a corresponding control program running in LabVIEW.

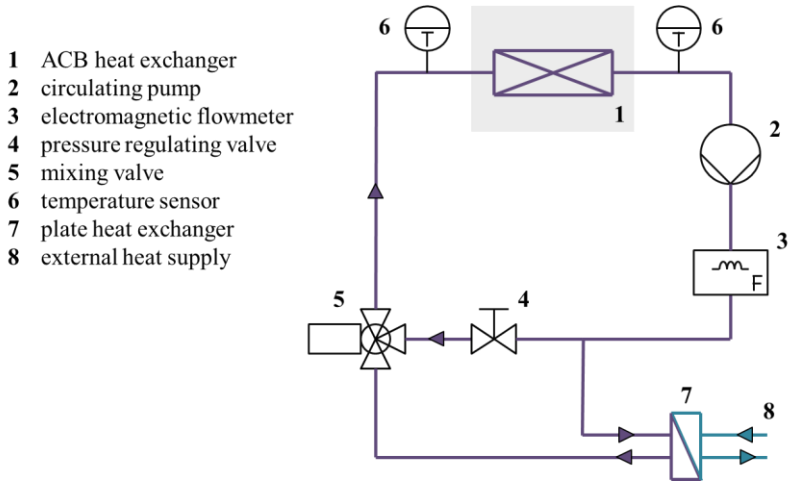

Fig. 2 Schematic of the hydraulic supply unit of the experimental setup

2.2 Measurement techniques and uncertainties

The instantaneous entrainment ratio I_e is determined by converting the measured values of the differential pressures $\Delta p_{orifice}$ at the corresponding orifice plates into primary and secondary air mass flows, respectively. Mass flow $\dot{m}$ is calculated as

$$\dot{m} = \gamma \cdot \sqrt{2 \cdot \Delta p_{orifice} \cdot \rho}, \tag{1}$$

where γ is a factor describing the geometry of the orifice and ρ is the air density. The changes of state for different flow and boundary conditions have to be considered. In a calibration process, ISO 5167-2 standard orifices were placed downstream the blowers. A positive leakage flow into the blower housing was observed and is taken into account in subsequent measurements by using the calibration data. Absolute pressure, relative humidity and air temperatures were measured using a digital flow meter (Testo 480) to determine fluid densities during the calibration process.

For the measurements, temperature sensors (Pt100, 1/10 EN 60751 Class B) are placed upstream the primary and secondary air inlets of the ACB in order to compensate for density changes due to heat input of the blower which was observed to be significant during the calibration process and nonlinearly dependent on the rotational speed of the blower. In Fig. 3 measured values of the air inlet temperature $T_{air,in}$ for the primary and the

secondary air, respectively, are shown for two different set-point primary air volumetric flow rates $\dot{V}_p$ together with the corresponding secondary air volumetric flow rates for steady-state conditions. Two observations are made. Firstly, high volumetric flow rates lead to inlet temperature increases of more than 3 K due to the heat input of the blower. Secondly, the laboratory space is large enough to ensure sufficiently stable temperature inflow conditions over a single set-point measurement time of 300 s.

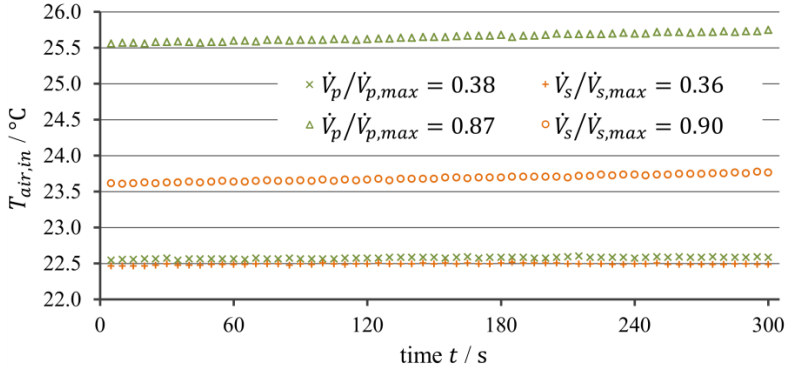

Fig. 3 Measured air inlet temperatures during two different measurements

Using (1), for a given orifice geometry ($\gamma = const.$) and given orifice differential pressure $\Delta p_{orifice}$ the measured mass flow $\dot{m}_{meas}$ is correlated with the measured calibration mass flow $\dot{m}_{cal}$ using the ratio of the corresponding air densities during calibration ρ_{cal} and measurements ρ_{meas} as follows

$$\dot{m}_{meas} = \dot{m}_{cal} \cdot \sqrt{\frac{\rho_{meas}}{\rho_{cal}}}. \tag{2}$$

In the water cycle two temperature sensors (Pt100, 1/10 EN 60751 Class B) are located closely at the heat exchanger inlet and outlet to measure the ACB water supply temperature $T_{water,in}$ and the ACB water return temperature $T_{water,out}$, respectively. Thermal power on the water side is evaluated according to

$$\dot{Q}_{th} = \dot{m}_{water} \cdot \bar{c}_{p,water} \cdot \left(T_{water,in} - T_{water,out}\right) \tag{3}$$

assuming an average specific heat $\bar{c}_{p,water}$ based on the measured ACB water temperatures and a constant absolute pressure in the hydraulic system.

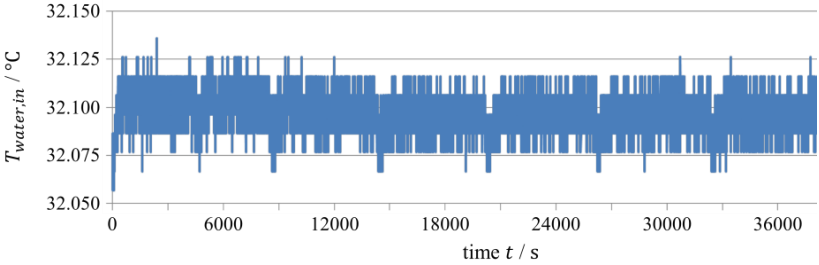

Fig. 4 Measured temperature fluctuation for a set heat exchanger water supply temperature

In Fig. 4 an exemplary plot of the measured ACB water supply temperature $T_{water,in}$ is shown for a controlled set-point temperature of 32.1 °C and a measurement frequency of 1 s^{-1}. The desired set-point is maintained accurately with fluctuations in the order of the measurement uncertainty of the temperature sensors.

Taking into consideration all measurement uncertainties specified for the measurement equipment an overall measurement uncertainty below 3% of the measured value can be estimated for the entrainment ratio I_e and an overall measurement uncertainty below 2% of the measured value can be estimated for the thermal power $\dot{Q}_{th}$ on the hydraulic side of the heat exchanger. All actual measurement values are gained using a sample rate of approx. 100 ms^{-1} and are processed as an average over the last ten values. Actual repeatability of the measured values is superior to the uncertainty which is shown in the results section.

3. Results and Discussion

Measurements of the thermal power $\dot{Q}_{th}$ and the entrainment ratio I_e were conducted for varying primary air mass flow rates $\dot{m}_p$. Values are time-averaged over a period of 300 s after a settling time of approx. 15 minutes for each measurement point was respected in order to ensure sufficiently stable thermal boundary conditions. Results are plotted using normalized values. Due to the upturned position of the ACB and the corresponding buoyancy effects the cooling mode is investigated using heat exchanger temperatures above the ambient air temperature.

In a first step, the influence of the secondary air hood (see Fig. 1) on the thermal power of the ACB was investigated. In Fig. 5 (top) results are shown for a constant water mass flow $\dot{m}_{water}$ and a constant temperature difference of $\Delta T = 10$ K between the water supply temperature $T_{water,in}$ and the secondary air inlet temperature T_{air,in_s}. In general, increasing $\dot{Q}_{th}$ can be observed for increasing $\dot{m}_p$. When the secondary air hood is removed thermal power is higher than in the two cases using the hood for

measurements A and B. Since deviations increase steadily with increasing primary air mass flow it seems likely that their origin is due to different secondary air approaching flow conditions between the two configurations. However, when looking at the corresponding temperatures of the ambient air $T_{air,amb}$ and the secondary air at the ACB inlet T_{air,in_s} in Fig. 5 (bottom) it becomes obvious that further effects need to be considered. Inlet temperature and ambient temperature are similar in the case without the hood, whereas the secondary air inlet temperature becomes increasingly higher for higher air mass flows when supplied to the hood by the secondary air blower in measurements A and B.

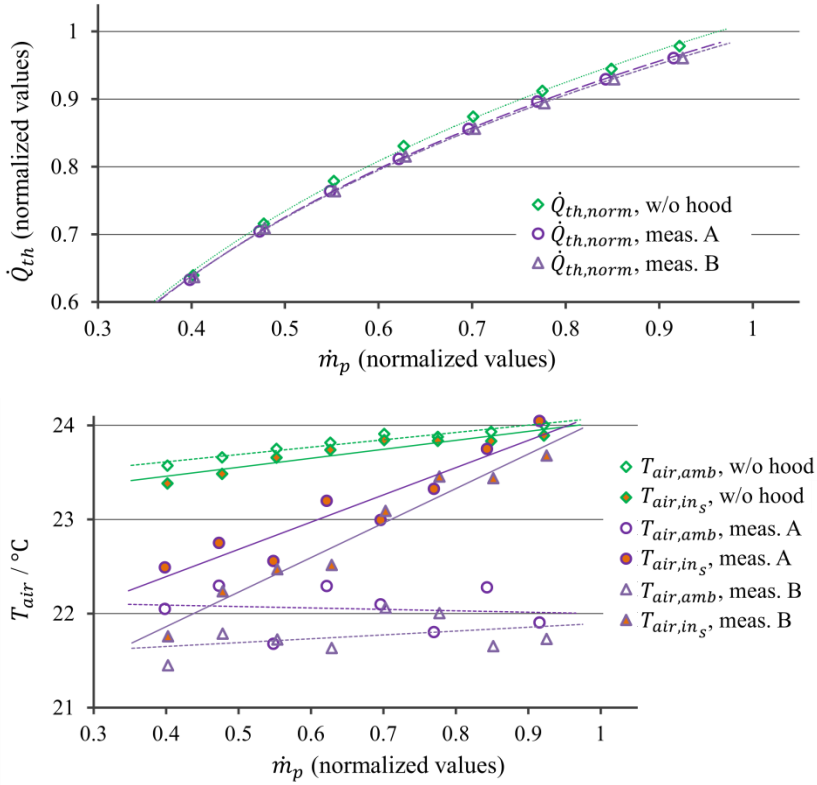

Fig. 5 Comparison of the measured thermal power (top) and corresponding average ambient air and secondary air inlet temperatures for each measurement point (bottom), $\Delta T = 10$ K.

Temperature measurements at the primary air nozzle exit plane revealed that heat transfer inside the ACB affects the primary air temperature downstream the ACB inlet. When the primary air volumetric flow rate at the

ACB inlet is controlled to remain at a constant value, the actual volumetric flow at the nozzle exit plane is altered depending on the temperature differences of the primary air, the secondary air, the ambient air and the water supply temperature. This results in higher or lower momentum primary air jets and an overestimation or underestimation of the measured entrainment ratios, respectively. Deviations in the thermal power between the two configurations with and without using the hood may be affected by a momentum loss by cooling of the primary air.

Comparing the results to the corresponding curve fits, average measurement repeatability below 0.5% and reproducibility below 2% can be stated for the thermal power measurements.

In order to investigate the influence of thermal boundary conditions on the entrainment ratio, measurements A and B are compared to results from measurements C using three different temperature differences ΔT between the water supply temperature and the secondary air inlet temperature. Results are shown in Fig. 6. In agreement with the results from the thermal power measurements a general increase in the entrainment ratio can be observed for increasing primary air mass flow rates. Measurements A, B and C2 show different results for the same temperature difference of $\Delta T = 10$ K.

Since the mass flow of the secondary air is measured before entering the ACB it can be expected that, given a constant primary air mass flow, the entrainment ratio I_e decreases for increasing ΔT because the entrained volumetric flow rate is constant while the specific volume of the secondary air increases. This is confirmed by the results of measurements C shown in Fig. 6 (top). Entrainment rates for $\Delta T = 5$ K are approx. 1% higher than entrainment rates for $\Delta T = 15$ K.

Assuming constant absolute pressure the density of the secondary air after passing the heat exchanger ρ_{HE,out_s} can be calculated as

$$\rho_{HE,out_s} = \rho_{air,in_s} \cdot \frac{T_{air,in_s}}{T_{air,in_s}+\Delta T_{air}}, \tag{3}$$

with the temperature difference caused by the heat exchanger

$$\Delta T_{air} = \frac{\dot{Q}_{th}}{c_{p,air} \cdot \dot{m}_s}, \tag{4}$$

using the measured values for the thermal power $\dot{Q}_{th}$, the secondary air mass flow rate $\dot{m}_s$ and the secondary air inlet temperature T_{air,in_s}. In order to exclude the effect of the different secondary air densities due to different thermal powers the resulting secondary air volumetric flow rates downstream the heat exchanger are related to the corresponding measured primary air mass flows divided by a reference density ρ_{ref} yielding

$$I_e{}^v = \frac{\dot{V}_{HE,out_S}}{\dot{m}_p \cdot (\rho_{ref})^{-1}}. \quad (5)$$

Results of the comparison using $I_e{}^v$ are shown in the bottom part of Fig. 6. It can be seen that the results of measurements C1, C2 and C3 converge to a single value which supports the assumptions made for (5).

Measurements were obtained under different boundary conditions. Absolute ambient pressure was varying from 98600 Pa in case A to 99400 Pa in case B to 100400 Pa in cases C while humidity and temperature of the ambient air were similar. When comparing the results of cases A, B and C2 no straightforward explanation for the deviations is found from the analysis of the condition of the ambient air.

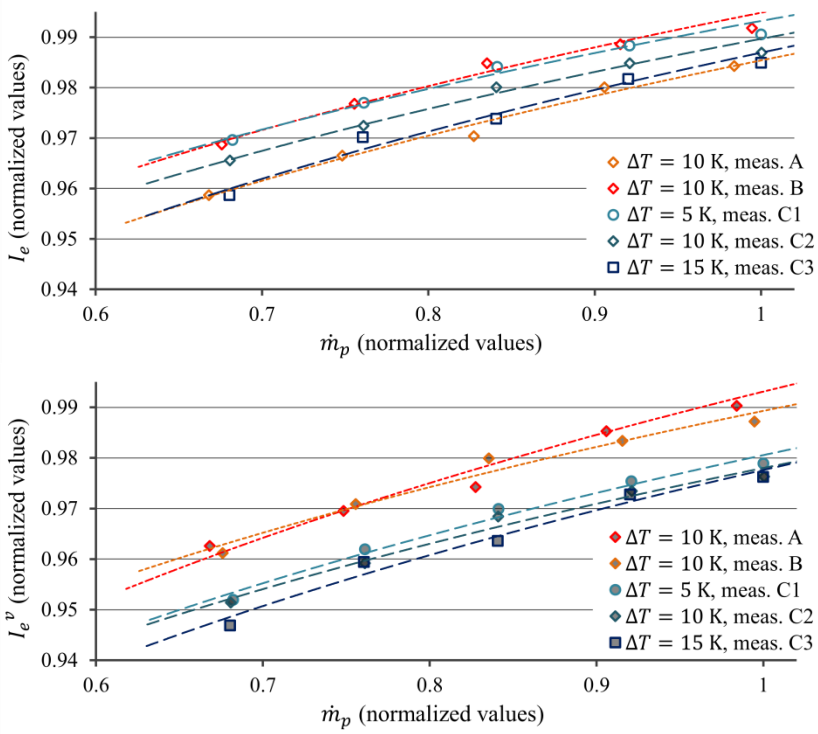

Fig. 6 Comparison of the entrainment ratio I_e (top) and the entrainment ratio based on the volumetric flow $I_e{}^v$ (bottom) for three different temperature differences

Average measurement repeatability below 0.2% of the measured value is obtained for the measurement of the entrainment ratio when comparing the

results to the corresponding curve fits. Reproducibility mainly depends on the absolute pressure of the ambient air resulting in variations below 2%.

4. Conclusions and Outlook

Results show sensitivities towards variations in the isothermal boundary conditions, for example when using upstream secondary air flow resistances due to the use of a secondary air measurement hood. Under non-isothermal boundary conditions deviations in the entrainment ratio due to variations of the heat exchanger supply temperature are found. A tendency of decreasing entrainment for increasing temperature differences ΔT is observable although density-corrected entrainment ratios apparently approach a single value under similar ambient conditions. Detailed local temperature measurements would be necessary in order to cover all interdependent thermal effects influencing the entrainment ratio. Partly oppositional behavior is expected when the ACB is operated not under conditions used in this study but under conditions intended by its design, meaning that the gravity vector is opposed to the main direction of secondary air inlet flow and the heat exchanger is supplied with cold water.

The experimental setup used in this study makes it possible to measure small variations in the entrainment rate of an active chilled beam over time with high accuracy and reproducibility. For best comparisons between different ACB geometries the analysis of the thermal power in the water cycle under constant ambient conditions is recommended.

Based on the results of this study it can be concluded that ACB geometry optimizations based on different flow patterns due to higher-than-usual water supply temperatures, e.g. when using geothermal heat sources for indoor cooling, are not necessary.

Acknowledgment

Grateful acknowledgment is made for financial support by Trox GmbH.

References

[1] F. P. Ricou, D. B. Spalding. Measurements of entrainment by axisymmetrical turbulent jets. J. Fluid Mech., pp. 21-32, 1961.
[2] P. E. Dimotakis, R. C. Miake-Lye, D. A. Papantoniou. Structure and dynamics of round turbulent jets, Phys. Fluids 26 (11), pp. 3185-3192, 1983.
[3] S. Chhabra, T. N. Shipman, A. K. Prasad. The entrainment behavior of a turbulent axisymmetric jet in a viscous host fluid, Exp. Fluids 38 (2005), pp. 70-79.
[4] H. Freitag, M. Schmidt, D. Müller, H. Koskela, P. Mustakallio. Particle image velocimetry measurements of the internal air flow in active chilled beams, Roomvent 2014, Sao Paolo, Brazil, October 2014.
[5] H. Koskela, P. Saarinen, H. Freitag, M. Schmidt, D. Müller, P. Mustakallio. LES simulation of the active chilled beam flow pattern, Roomvent 2014, Sao Paolo, Brazil, October 2014.
[6] P. Mathis et al. Heat removal in shopping centers with high cooling loads by air-water systems with small fresh air amount and high cold water supply temperature, Ventilation 2015, Shanghai, China.